LAWRENCE
LIVERMORE
NATIONAL
LABORATORY

UCRL-PROC-208022

Effect of Surface Stress Mitigation on the Corrosion Behavior of Alloy 22

David V. Fix, Ahmet Yilmaz, Lana L. Wong, John C. Estill, Raúl B. Rebak

November 16, 2004

CORROSION/2005 and NACE Expo
Houston, TX, United States
April 3, 2005 through April 7, 2005

09Nov04
Paper 05606 prepared to be presented during the CORROSION/2005 Conference, 3-7 April 2005 in Houston, TX

EFFECT OF SURFACE STRESS MITIGATION ON THE CORROSION BEHAVIOR OF ALLOY 22

David V. Fix, Ahmet Yilmaz, Lana L. Wong, John C. Estill
and Raúl B. Rebak
Lawrence Livermore National Laboratory, Livermore, CA, 94550

ABSTRACT

When metallic plates are welded, for example using the Gas Tungsten Arc Welding (GTAW) process, residual tensile stresses may develop in the vicinity of the weld seam. Processes such as Low Plasticity Burnishing (LPB) and Laser Shock Peening (LSP) could be applied locally to eliminate the residual stresses produced by welding. In this study, Alloy 22 (N06022) plates were welded and then the above-mentioned surface treatments were applied to eliminate the residual tensile stresses. The aim of the current study was to comparatively test the corrosion behavior of as-welded (ASW) plates with the corrosion behavior of plates with stress mitigated surfaces. Immersion and electrochemical tests were performed. Results from both general and localized corrosion tests show that the corrosion resistance of the mitigated plates was not affected by the surface treatments applied.

Keywords: N06022, Gas Tungsten Arc Welding, Stress Mitigation, Burnishing, Laser Peening

INTRODUCTION

Alloy 22 (N06022) has nominally 56% Nickel (Ni), 22% Chromium, 13% Molybdenum (Mo) and 3% Tungsten (W). [1] Alloy 22 is highly resistant to all types of corrosion, including environmentally assisted cracking, localized corrosion such as crevice corrosion and general or uniform corrosion. [2-4] Alloy 22 was selected for the fabrication of the outer shell of the high level nuclear waste containers for the proposed Yucca Mountain repository. [5-6] The containers will be fabricated and solution heat treated before the waste is loaded into the containers. [6] After loading, the closure lid of the Alloy 22 containers will be welded using the gas tungsten arc welding (GTAW) process. [7] There are currently two methods under consideration to minimize or eliminate residual tensile stresses that may result from the final closure welding. These are: (1) Low Plasticity Burnishing (LPB) and (2) Laser shock Peening (LSP). These stress mitigation treatments are aimed to reducing residual surface tensile stresses that could promote the initiation of environmentally assisted cracking (EAC) in Alloy 22. [6]

It is important to know if the proposed surfaced treatments will affect the general and localized corrosion resistance of welded plates. The aim of this work was to evaluate comparatively the general and localized corrosion resistance of Alloy 22 in as-welded (ASW) plates and in welded plates that were treated for surface stress mitigation. Immersion and electrochemical tests were performed to assess changes in the corrosion resistance of the three studied materials.

EXPERIMENTAL PROCEDURES

Again, coupons and specimens were prepared from three differently treated welded plates of Alloy 22. Both immersion and electrochemical tests were conducted following ASTM standards. [8]

As-Welded (ASW) Plates

Two 1-inch thick Alloy 22 plates (Heat XX2246BG) were GTAW welded lengthwise using 0.045-inch thick Alloy 22 wire (XX2048BG) for filler metal. Before the weld joining, each plate was approximately 16-inch long and 6-inch wide.

The ASW plate used for corrosion testing was called F6 and the coupons and specimens prepared from this plate were all named starting with the letter W.

Low Plasticity Burnishing (LPB)

LPB is a process by which a smooth hard ball is rolled over the surface of the metal to be burnished imparting compressive deformation. [9-10] The treatment in the studied Alloy 22 welded plates was performed in two steps using balls of two different sizes, the larger one with an effective surface area of 0.0154 inch² and the smaller one with an effective surface area of 0.00067 inch². In the first step the larger ball was rolled at a pressure of 780 ksi to create compressive stresses to a larger depth. In the second step, the smaller ball was rolled at a pressure of 821 ksi to increase the level of compressive stresses near the surface. The LPB treatment of the Alloy 22 studied plates was carried out at the Surface Enhancement Technologies Company in Cincinnati, Ohio.

The burnished plate was called F4 and the coupons and specimens prepared from this plate were all named starting with the letter B.

Laser Shock Peening (LSP)

Laser shock peening is a process by which a laser beam is pulsed upon a metallic surface producing a planar shockwave that travels though the work piece and plastically deforms into compressive stresses a layer of material. [11-12] The laser beam is generally applied to the work piece though a transparent overlay and an absorbent coating. A plasma forms under the overlay increasing the pressure and therefore the compressive stresses on the treated part. It has been shown specifically that a LSP treatment of 33-mm thick Alloy 22 welds actually produced a 4-mm deep layer of compressive stresses on the surface. [12] The current LSP treatment in the Alloy 22 welded plates was performed by applying laser pulses of 14 Joules for 25 nano seconds. Each spot dimension was approximately 2.5 mm square.

The laser-peened plate was called F2 and the coupons and specimens prepared from this plate were all named starting with the letter P.

IMMERSION CORROSION TESTS

Preparation of the Immersion Coupons

Three types of welded plates were studied: (1) As-Welded (ASW), (2) Welded plus LPB and (3) Welded plus LSP. Table 1 shows the heats and the chemical composition of the plates. The plates met the specifications of ASTM B 575. [1] The plates were cut in approximately 0.5-inch thick slices perpendicular to the weld seam. There were two LPB plate slices (B9 and B10), three LSP plate slices (P13, P14 and P15) and three ASW plate slices (W13, W14 and W15). The immersion corrosion testing coupons were prepared from the above listed plate slices. The testing coupons were approximately 0.5 to 1-inch wide, 0.25 to 0.5-inch thick and 2-inch long. The 2-inch length contained the weld seam at the center and base metal at both sides of the weld seam. These sizes were constrained by the testing apparatus (ASTM G 28). [8] The surface area of the coupons varied generally from 20 to 40 cm² and the weight varied from 40 to 90 g. The coupons were degreased in acetone, rinsed in de-ionized water and let dry. Each coupon was dimensioned and weighed three times before the corrosion testing started.

ASTM G 28 A or Ferric Sulfate + Sulfuric Acid Test

This method measures the susceptibility of nickel alloys to intergranular attack. It is often used to determine preferential intergranular attack near welds or in heat affected zones (HAZ). The guidelines are specified in the Annual Book of ASTM standards. [8] Figure 1 shows the setting for the tests. The ASTM G 28 A method for Alloy 22 consists in immersing coupons of the alloy for 24 h in a boiling solution of 42 g/L $Fe_2(SO_4)_3$ (ferric sulfate) plus 50% H_2SO_4 (sulfuric acid). The difference in the mass of the coupon between before and after the test can be used to calculate the uniform corrosion rate. Corrosion rates were calculated according to Equation 1 [8]

$$CR(mm/year) = 8.76 \times 10^4 \frac{\Delta W(g)}{A(cm^2) \cdot t(h) \cdot d(g \cdot cm^{-3})} \qquad (1)$$

Where ΔW is the difference if weight of the coupon between before and after the test, A is the surface area of the coupon, t is the testing time (24 h) and d is the density of Alloy 22 (8.69 g/cm³). [8]
The testing coupons were parallelepipeds, that is, they had six faces. Only one face is of interest (the treated one, which was either ASW, LPB or LSP). The other faces are as-cut faces and remained in the same condition for all three types of coupons. Whenever comparing surface characteristics after corrosion only the face of interest is discussed. Figure 2 shows the general appearance of three coupons after immersion testing. These coupons represent each one of the testing materials.

Preparation of the Electrochemical Specimens

Alloy 22 specimens were mainly prepared from 1-inch thick plate. Table 1 gives the heats and the chemical composition of the material for the tested specimens. The specimens were prism crevice assemblies (PCA) (Figure 3) as reported elsewhere. [13] For the current tests, the surface area of the PCA specimens was 3.27 cm². The original surface of a PCA specimen is usually 14.06 cm². [13] However for the current specimens, all the non-important surfaces were lacquered to avoid their interaction with the

environment. Thus, only the ASW, LPB and LSP surfaces were exposed to the electrolyte solution for the tests. The crevicing mechanism for these PCA tests was based on ASTM G 48 12-tooth washer; however the washer was not the standard ceramic plus PTFE tape used in other tests at LLNL. [13] Since the current specimens did not have a completely smooth flat surface the crevicing washer was constructed using a hard organic material (PVDF or Polyvinylidene fluoride), which could sufficiently deform and provide a tight crevicing mechanism on an uneven surface. The PVDF washers were also coated with PTFE tape in a similar way as the ceramic washers. The PCA specimens were degreased in acetone and DI water, let dry and then all the non-important surfaces were lacquered. The lacquer was allowed to dry for at least 6 hours and then the specimens were inspected for discontinuities. The resistance of the lacquered surfaces was measured to verify electrical insulation from the electrolyte. The specimens were also inspected after the tests confirming that the lacquer did not break or disbond during testing. Specimens were used in the as-welded (ASW), in the low plasticity burnishing (LPB) and in the laser shock peened (LSP) conditions. The specimens were labeled respectively W, B and P. The weld seam run across center of the surface of the specimen that was purposely creviced with the multiple teeth washer (Figure 3).

Electrolyte Solutions and Testing Procedures

Electrochemical tests were performed in deaerated simple salt solutions. These solutions were 1 M NaCl pH 6 at 90°C and 6 m NaCl + 0.9 m KNO_3 pH 5.5 at 80°C and 100°C. The second solution has a $[Cl^-]/[NO_3^-]$ ratio of 6.67. Nitrogen (N_2) was purged through the solution at a flow rate of 100 cc/min for 24 hours while the corrosion potential (E_{corr}) was monitored. Nitrogen bubbling was carried throughout all the electrochemical tests. The electrochemical tests were conducted in a one-liter, three-electrode, borosilicate glass flask (ASTM G 5). [8] A water-cooled condenser combined with a water trap was used to avoid evaporation of the solution and the ingress of air. The temperature of the solution was controlled by immersing the cell in a thermostatisized silicone oil bath. All the tests were carried at ambient pressure. The reference electrode was saturated silver chloride (SSC) electrode, which has a potential of 199 mV more positive than the standard hydrogen electrode (SHE). The reference electrode was connected to the solution through a water-jacketed Luggin probe so that the electrode was maintained at near ambient temperature. The counter electrode was a flag (36 cm^2) of platinum foil spot-welded to a platinum wire. All the potentials in this paper are reported in the SSC scale.

Basically, the test sequence for each specimen consisted of three parts: (1) E_{corr} evolution as a function of time for 24 h, (2) Polarization Resistance (ASTM G 59) three subsequent times and (3) A larger anodic polarization to determine susceptibility to crevice corrosion. The larger anodic polarization was conducted using Cyclic Potentiodynamic Polarization (CPP) method (ASTM G 61).

Polarization Resistance (ASTM G 59)- Corrosion rates (CR) were obtained using the polarization resistance method (ASTM G 59). [8] Each one of these tests lasts approximately four minutes. An initial potential of 20 mV below the corrosion potential (E_{corr}) was ramped to a final potential of 20 mV above E_{corr} at a rate of 0.167 mV/s. Linear fits were constrained to the potential range of 10 mV below E_{corr} to 10 mV above E_{corr}. During the fitting of the data to calculate the polarization resistance (Rp), the potential (E) was plotted in the X-axis. The Tafel constants, b_a and b_c, were assumed to be $\pm$ 0.12 V/decade. Corrosion rates were calculated using Equation 2

$$CR(nm/yr) = k\frac{i_{corr}}{\rho}EW \qquad \textbf{(2)}$$

Where k is a conversion factor (3.27 x 10^9 nm·g·A^{-1}·cm^{-1}·yr^{-1}), i_{corr} is the measured corrosion current density in A/cm^2, EW is the equivalent weight, and ρ is the density of Alloy 22 (8.69 g/cm^3). Assuming an equivalent dissolution of the major alloying elements as Ni^{2+}, Cr^{3+}, Mo^{6+}, Fe^{2+}, and W^{6+}, the EW for Alloy 22 is 23.28 (ASTM G 102). [8]

Cyclic Potentiodynamic Polarization - CPP (ASTM G 61)- The test to assess the susceptibility of Alloy 22 to localized corrosion and passive stability was the cyclic potentiodynamic polarization technique, CPP (ASTM G 61). [8] The potential scan was started 100 mV below E_{corr} at a set scan rate of 0.167 mV/s. The scan direction was reversed when the current density reached 5 mA/cm^2 in the forward scan. Depending on the range of applied potentials, each CPP test could last between 1 h and 3 h. From the polarization curve, several parameters of importance can be extracted. The E20 and E200 represent values of breakdown potential and ER10, ER1 and ERCO represent values of repassivation potential.

EXPERIMENTAL RESULTS

Immersion Corrosion Tests

Table 2 shows the corrosion rate results from the immersion testing. For all three types of coupons (ASW, LPB and LSP) the corrosion rate was the same. The highest average corrosion rate corresponded to the ASW coupons and the lowest to the LSP coupons but considering the standard deviation (SD), the corrosion rate values are indistinguishable from each other. Besides the data reported on Table 2, the corrosion rate of the base metal of the plates (away from the weld) in ASTM G 28 was also measured. The corrosion rate of the base metal was found to be 1.83 mm/year, which was higher than that of any of the welded coupons. It has been previously reported that the corrosion rate of as-welded 0.125-inch thick sheets of Alloy 22 in ASTM G 28A was 1.08 mm/year. [14] The standard corrosion rate of Alloy 22 given in a commercial brochure is 1.016 mm/year. [2] The common acceptance criterion for the maximum allowed corrosion rate for Alloy 22 is 80 mpy or 2 mm/year. [15]

After the corrosion immersion tests each specimen was thoroughly inspected under optical microscopy (stereomicroscope). Results are given in Table 3. All three type of materials suffered intergranular attack (IGA) in the heat affected zone (HAZ). Figure 2 shows macrograph images of characteristic tested coupons. The obvious IGA in the HAZ appears as black strips on each side of the weld seam (Figure 2). The IGA in the HAZ seemed less defined in the LSP coupons than in the ASW coupons.

Figures 4-5 show the aspect of the ASW corroded coupons, both in the base metal. Figure 4 represents the base metal away from the weld seam, which is the part of the plate that was not affected by the welding process. Figure 2 shows shallow and sporadic IGA. Figure 5 shows the aspect of corrosion in the HAZ, which is a couple of millimeters from the edge of the weld seam. Figure 5 shows more pronounced IGA probably promoted by second phase precipitation due to the exposure of the HAZ to intermediate temperatures (600 to 900°C) for the time involved in the welding process. [14-15]

Figures 6-7 show the aspect of the LPB corroded coupons, both in the base metal. Figure 6 represents the base metal away from the weld seam, which is the part of the plate that was not affected by the welding process. Figure 6 shows shallow and sporadic IGA, same as in the ASW coupon (Figure 4). Figure 7 shows the aspect of corrosion in the HAZ, which is a couple of millimeters from the weld seam. Figure 7 shows more pronounced IGA than in the base metal away from the weld. This was probably promoted by second phase precipitation due to the exposure of the HAZ to intermediate temperatures (600 to 900°C) for the time involved in the welding process. [14-15] The aspect of Figure 7 is

similar to that of Figure5 showing that LPB treatment did not decrease the corrosion characteristics of an untreated welded plate (ASW).

Figures 8-9 show the aspect of the LSP corroded coupons, both in the base metal. Figure 8 represents the base metal away from the weld seam, which is the part of the plate that was not affected by the welding process. Figure 8 shows shallow and sporadic IGA, same as in the ASW and LPB coupons (Figures 4 and 6). Figure 9 shows the aspect of corrosion in the HAZ, which is a couple of millimeters from the edge of the weld seam. Figure 9 shows a type of attack that is less pronounced IGA and more type of enhanced general corrosion. It appears that the localized corrosion in the HAZ was different in the LSP coupon (Figure 9) than in the ASW and LPB coupons (Figures 5 and 7). At this moment it cannot be speculated what mechanism could have changed the mode of attack of the LSP coupons.

RESULTS FROM THE ELECTROCHEMICAL TESTS

The Corrosion Potential

Table 3 shows the average E_{corr} for the three types of material after 24-hour immersion in deaerated 1 M NaCl at 90°C. Table 3 shows that the E_{corr} was the same for all three materials ASW, LPB and LSP. Table 4 lists the average E_{corr} values in deaerated 6 m NaCl + 0.9 m KNO_3 at 80°C and 100°C. For the LPB specimens only data at 100°C is available due to the limited number of specimens available for testing. For both the ASW and LSP specimens, as the temperature increased from 80°C to 100°C, the E_{corr} slightly decreased. This is expected since at higher temperatures metals tend to become more active in saline solutions. Table 4 also shows that at 100°C the E_{corr} of all three materials (ASW, LPB and LSP) was the same and between –238 mV and –272 mV SSC. According to the values of E_{corr}, all the materials behaved similarly when immersed in hot saline solutions.

The Corrosion Rate from Rp Measurements

Tables 3 and 4 show the corrosion rates of all three tested materials (ASW, LPB and LSP) in deaerated 1 M NaCl and in 6 m NaCl + 0.9 m KNO_3 solutions, respectively. Table 3 shows that the average corrosion rate of all the tested material in 1 M NaCl solution varied between 0.188 μm/year for the LPB specimens and 0.330 μm/year for the LSP specimens. The LSP average corrosion rate was the highest due to the abnormally high corrosion rate values of specimen P2. Considering standard deviations, the corrosion rate values for ASW, LPB and LSP cannot be differentiated from each other (Table 3).

Table 4 shows the average corrosion rates for the three materials in 6 m NaCl + 0.9 m KNO_3 at 80°C and 100°C. The effect of the temperature on the corrosion rate cannot be fully quantified since there are specimens that gave corrosion rates that may be result of anomalous behavior (e.g. W3, W4 and P3). Considering the corrosion rate of all the materials at 100°C, and ignoring the anomalous behaviors, the corrosion rate values fluctuated between 0.18 μm/year for LSP and 0.21 μm/year for the ASW specimens. These values can be considered practically the same. That is, in both electrolyte solutions all materials behaved the same regarding corrosion rate measures using ASTM G 59.

Cyclic Potentiodynamic Polarization (CPP)

Figure 10 shows the cyclic potentiodynamic polarization curves for the three tested materials in deaerated 1 M NaCl pH 6 at 90°C. Figure 10 shows that the behavior of all these materials was practically the same. Similarly, Figure 11 shows the cyclic potentiodynamic polarization curves for the three tested materials in deaerated 6 m NaCl + 0.9 m KNO_3 pH 5.5 at 100°C. Again, the polarization curves are the same for the ASW, LPB and LSP materials in the chloride plus nitrate brine.

Table 4 shows the effect of the temperature on the breakdown and repassivation potential for ASW and LSP materials (LPB was not tested at 80°C). As the temperature increased from 80°C to 100°C, both the breakdown and repassivation potentials slightly decreased as it may be expected. Figures 12 and 13 show E_{corr} and the parameters from the CPP curves (listed in Tables 3 and 4) for 1 M NaCl at 90°C and for 6 m NaCl + 0.9 m KNO_3 at 100°C, respectively. For the 1 M NaCl solution (Table 3 and Figure 12), the breakdown potentials (E20 and E200) seemed slightly higher for LPB than for ASW and LSP materials. However, the repassivation potentials (ER1 and ERCO) seemed higher for the ASW material. In the 6 m NaCl + 0.9 m KNO_3 solution (Table 4 and Figure 13), the breakdown potentials (E20 and E200) seemed slightly higher for LPB than for ASW and LSP. However, the repassivation potentials (ER1 and ERCO) seemed higher for the LSP material. The difference in potential values between the three materials is small enough to be considered within experimental error. For example, in the 6 m NaCl + 0.9 m KNO_3 solution at 100°C, the difference between the values of E200 is smaller than 10 mV between one type of material and another (Table 4).
Figures 14-19 show the appearance of the specimens used for cyclic potentiodynamic polarization after the tests in 1 M NaCl at 90°C. When creviced Alloy 22 is polarized to high anodic potentials (Figure 10) the specimens may suffer crevice corrosion. Figures 14-15 show the mode of crevice corrosion attack in ASW specimen W6. This is a typical type of crevice corrosion for Alloy 22 in 1 M NaCl at 90°C solution. [13] Figure 14 also shows that the ASW specimen was not totally flat since it was not finished with 600 grit paper as in previous tests. [13] Figure 15 shows a detail of the crevice corrosion attack in Figure 14, where a characteristic dendritic structure of the weld seam can be seen. Similar findings are for LPB specimen B3 (Figures 16-17) and for LSP specimen P5 (Figures 18-19). Basically, Figures 14-19 show that the mode of crevice corrosion attack does not change if the ASW plate is LPB or LSP treated.

Table 5 shows a comparison between the data in Table 3 and 4 with data known from previous publications for other tested Alloy 22 specimens in the same electrolytes. In spite that the referenced data [13,16] was developed for freshly ground paper 600 and fully exposed (not lacquered) creviced specimens, the repassivation potentials in each environment (pure chloride and chloride plus nitrate) are practically the same. This observation (Table 5) not only demonstrates that stress mitigated materials behave electrochemically the same as as-welded materials but also gives confidence that the testing methods used here provide accurate and reproducible parameters to compare the behavior of different materials.

CONCLUSIONS

(1) Surface tensile stress mitigation processes such as low plasticity burnishing (LPB) and laser shock peening (LSP) do not affect the corrosion resistance of welded Alloy 22 plates.

(2) Immersion tests in standard G 28 A solution showed that the corrosion rate by weight loss was the same for as-welded (ASW) material as for LPB and LSP materials

(3) Electrochemical tests such as cyclic potentiodynamic polarization showed that the anodic behavior of the three tested materials (ASW, LPB and LSP) was the same

(4) The repassivation potential in chloride solutions of the three materials was the same

(5) When corrosion occurred, the mode of attack of the three materials (ASW, LPB and LSP) remained the same.

ACKNOWLEDGMENTS

This work was performed under the auspices of the U. S. Department of Energy by the University of California Lawrence Livermore National Laboratory under contract N° W-7405-Eng-48. This work is supported by the Yucca Mountain Project, which is part of the Office of Civilian Radioactive Waste Management (OCRWM) of DOE

REFERENCES

1. ASTM International, Annual Book of ASTM Standards, Volume 02.04 “Non-Ferrous Metals” Standard 575 B (West Conshohocken, PA: ASTM International, 2002).
2. Haynes International, “Hastelloy C-22 Alloy”, Brochure H-2019E (Haynes International, 1997: Kokomo, IN)
3. R. B. Rebak in Corrosion and Environmental Degradation, Volume II, p. 69, Wiley-VCH, Weinheim, Germany (2000)
4. R. B. Rebak and P. Crook, *Advanced Materials and Processes*, February 2000
5. Yucca Mountain Science and Engineering Report, U. S. Department of Energy, Office of Civilian Radioactive Waste Management, DOE/RW-0539, Las Vegas, NV, May 2001
6. G. M. Gordon, Corrosion, 58, 811 (2002)
7. S. C. Lu, G. M. Gordon and P. L. Andresen, PVP-Vol. 483, Transportation, Storage and Disposal of Radioactive Materials (American Society of Mechanical Engineers, 2004: New York, NY)
8. ASTM International, Annual Book of ASTM Standards, Volume 03.02 “Wear and Erosion; Metal Corrosion” p. 91 (West Conshohocken, PA: ASTM International, 2004)
9. U.S. Patents 5,826,453 (Oct. 1998), 6,415,486 B1 (Jul. 2002)

10. P. S. Prevéy, R. A. Ravindranath, M. Shepard and T. Gabb "Case Studies of Fatigue Life Improvement Using Low Plasticity Burnishing in Gas Turbine Engine Applications," Proc. Of ASME Turbo Expo 2003, 16-19 June 2003, Atlanta, GA
11. C. S. Montross, T. Wei, L. Ye, G. Clark and Y.-W. Mai "Laser Shock Processing and its Effects on Microstructure and Properties of Metal Alloys: a Review," International Journal of Fatigue, 24, 1021-1036 (2002)
12. M. R. Hill, A. T. DeWald, L. A. Hackel, H.-L. Chen, R. C. Specht and F. B. Harris "Laser Peening Technology," Advanced Materials and Processes, 8, p. 65 (2003)
13. K. J. Evans, A. Yilmaz, S. D. Day, L. L. Wong, J. C. Estill and R. B. Rebak "Comparison of Electrochemical Methods to Determine Crevice Corrosion Repassivation Potential of Alloy 22 in Chloride Solutions," JOM, January 2005 (to be published)
14. R. B. Rebak, T. S. E. Summers, T. Lian, R. M. Carranza, J. R. Dillman, T. Corbin and P. Crook "Effect of Thermal Aging on the Corrosion Behavior of Wrought and Welded Alloy 22," Corrosion/2002, Paper 02542 (NACE International, 2002: Houston, TX)
15. R. B. Rebak, T. S. E. Summers and R. M. Carranza "Mechanical Properties, Microstructure and Corrosion Performance of C-22 Alloy Aged at 260°C to 800°C, Scientific Basis for Nuclear Waste Management XXIII, Vol. 608, p. 109 (Materials Research Society, 2000: Warrendale, PA)
16. G. O. Ilevbare, K. J. King, S. R. Gordon, H. A. Elayat, G. E. Gdowski and T. S. E. Summers "Effect of Nitrate on the Repassivation Potential of Alloy 22 in Chloride Containing Solutions," Fall 2004 Meeting of the Electrochemical Society, 0308Oct04, Honolulu, HI (to be published).

==========

RBR, 24Oct04

TABLE 1
CHEMICAL COMPOSITION IN WT% OF THE STUDIED MATERIALS

Element	**Plate or Base Metal Heat XX2246BG**	**Weld Wire or Filler Metal Heat XX2048BG**
Ni	~60	59.4
Cr	20.4	20.48
Mo	13.9	14.21
W	3.3	3.02
Fe	2.3	2.53
Co	0.2	0.02
Mn	0.2	0.2
V	0.01	0.02
Cu	---	0.04

TABLE 2
RESULTS FROM G 28 A IMMERSION CORROSION TESTS

Material	Coupon ID	Corrosion Rate, mm/year (mpy)	Average CR ± SD mm/year	Observations After the Tests
ASW	W13-S1	1.26 (49.6)	1.303 ± 0.040	IGA in HAZ, uneven attack in BM away from WS
ASW	W14-S1	1.31 (51.48)		
ASW	W15-S1	1.34 (52.72)		
LPB	B9-S2	1.37 (54.02)	1.295 ± 0.106	IGA in HAZ, deformation marks perpendicular to the WS (left by ball?)
LPB	B10-S2	1.22 (48.12)		
LSP	P13-S2	1.32 (52.07)	1.257 ± 0.055	IGA in HAZ, uneven attack on base metal lattice marks (left by LSP?)
LSP	P14-S2	1.23 (48.41)		
LSP	P15-S2	1.22 (47.86)		
CR = corrosion rate, SD = standard deviation, IGA = intergranular attack, HAZ = heat affected zone, BM = Base Metal, WS = Weld Seam				

TABLE 3
CHARACTERISTIC POTENTIALS (mV, SSC) AND CORROSION RATE (CR IN μm/YEAR)
OF ALLOY 22 IN 1 M NaCl SOLUTION AT 90°C

ID	Material	$E_{corr,}$ 24 h	Corrosion Rate	E20	E200	ER10	ER1	ERCO
W6	ASW	-286	0.22, 0.27, 0.21	374	567	-17	-88	-104
W7	ASW	-198	0.19, 0.15, 0.21	356	547	-17	-79	-91
Ave ± SD	ASW	-242 ± 44	0.208 ± 0.039	365 ± 9	557 ± 10	-17 ± 0	-84 ± 5	-98 ± 7
B3	LPB	-260	0.18, 0.15, 0.20,	480	706	-59	-123	-134
B4	LPB	-258	0.20, 0.21, 0.19	383	623	-10	-95	-111
Ave ± SD	LPB	-259 ± 1	0.188 ± 0.021	432 ± 49	665 ± 42	-35 ± 25	-109 ± 14	-123 ± 12
P2	LSP	-244	0.41, 0.51, 0.38	319	544	-14	-86	-104
P5	LSP	-195	0.22, 0.23, 0.23	381	575	-22	-100	-114
Ave ± SD	LSP	-220 ± 25	0.330 ± 0.121	350 ± 31	560 ± 16	-18 ± 4	-93 ± 7	-109 ± 5
ID = Specimen Identification, Ave ± SD = Average value ± standard deviation, E20 and E200 is the potential in the forward scan for which the current density reaches 20 and 200 μA/cm² respectively. ER10 and ER1 is the potential in the reverse scan for which the current density reaches 10 and 1 μA/cm² respectively. ERCO is the potential at which the reverse scan intercepts the forward scan (cross-over potential).								

TABLE 4
CHARACTERISTIC POTENTIALS (mV, SSC) AND CORROSION RATE (CR IN μm/YEAR)
OF ALLOY 22 IN 6 m NaCl + 0.9 m KNO_3 AT 80°C AND 100°C

	Material	$E_{corr,}$ 24 h	Corrosion Rate	E20	E200	ER10	ER1	ERCO
W1, 80	ASW	3	0.27, 0.26, 0.23	727	856	85	NA	NA
W3, 80	ASW	-38	0.74, 0.72, 0.75	798	867	285	-65	-31
Ave ± SD	ASW	-18 ± 21	0.495 ± 0.242	763 ± 36	862 ± 6	185 ± 100	-65 ± 0	-31 ± 0
W4, 100	ASW	-297	2.36, 2.1, 1.93	443	840	-26	-83	-83
W5, 100	ASW	-247	0.22, 0.21, 0.21	441	813	-29	-72	-81
Ave ± SD	ASW	-272 ± 25	1.172 ± 0.966	442 ± 1	827 ± 14	-28 ± 2	-78 ± 6	-82 ± 1
B1, 100	LPB	-251	0.19, 0.22, 0.20,	480	811	-35	-83	-19
B2, 100	LPB	-225	0.20, 0.19, 0.20	488	858	-31	-86	-95
Ave ± SD	LPB	-238 ± 13	0.200 ± 0.010	484 ± 4	835 ± 24	-33 ± 2	-85 ± 2	-57 ± 38
P4, 80	LSP	-183	0.14, 0.14, 0.16	659	858	588	-31	-59
P6, 80	LSP	-279	0.11, 0.15, 0.11	676	874	207	-14	-38
Ave ± SD	LSP	-231 ± 48	0.135 ± 0.019	668 ± 9	866 ± 8	398 ± 191	-23 ± 9	-49 ± 11
P1, 100	LSP	-265	0.17, 0.18, 0.19	443	827	-5	-68	-79
P3, 100	LSP	-248	0.52, 0.39, 0.86	436	830	-19	-77	-45
Ave ± SD	LSP	-257 ± 9	0.385 ± 0.248	440 ± 4	829 ± 2	-12 ± 7	-73 ± 5	-62 ± 17

ID = Specimen Identification, T = Temperature in °C, Ave ± SD = Average value ± standard deviation, E20 and E200 is the potential in the forward scan for which the current density reaches 20 and 200 μA/cm² respectively. ER10 and ER1 is the potential in the reverse scan for which the current density reaches 10 and 1 μA/cm² respectively. ERCO is the potential at which the reverse scan intercepts the forward scan (cross-over potential), NA = Not Available.

TABLE 5
COMPARISON BETWEEN THE AVERAGE CHARACTERISTIC POTENTIALS
OF CURRENT RESULTS AND ARCHIVE RESULTS FOR N06022

Material/ Data Source	ER1	ERCO	ER, CREV
1 M NaCl, 90°C			
ASW Current	-84 ± 5	-98 ± 7	NA
LPB Current	-109 ± 14	-123 ± 12	NA
LSP Current	-93 ± 7	-109 ± 5	NA
Archive MA MCA Ref. 13	-80 ± 19	-49 ± 16	-30 ± 8
Archive ASW MCA Ref. 13	NA	NA	-99 ± 9
6 m NaCl + 0.9 m KNO_3, 100°C			
ASW Current	-78 ± 6	-82 ± 1	NA
LPB Current	-85 ± 2	-57 ± 38	NA
LSP Current	-73 ± 5	-62 ± 17	NA
Archive ASW MCA Ref. 16	-49 ± 27	-63 ± 23	NA
MCA = Multiple Crevice Assembly (lollipop), ER,CREV obtained using the Tsujikawa-Hisamatsu Electrochemical (THE) Method			

FIGURE 1 - Setting for the ASTM G 28 A tests.

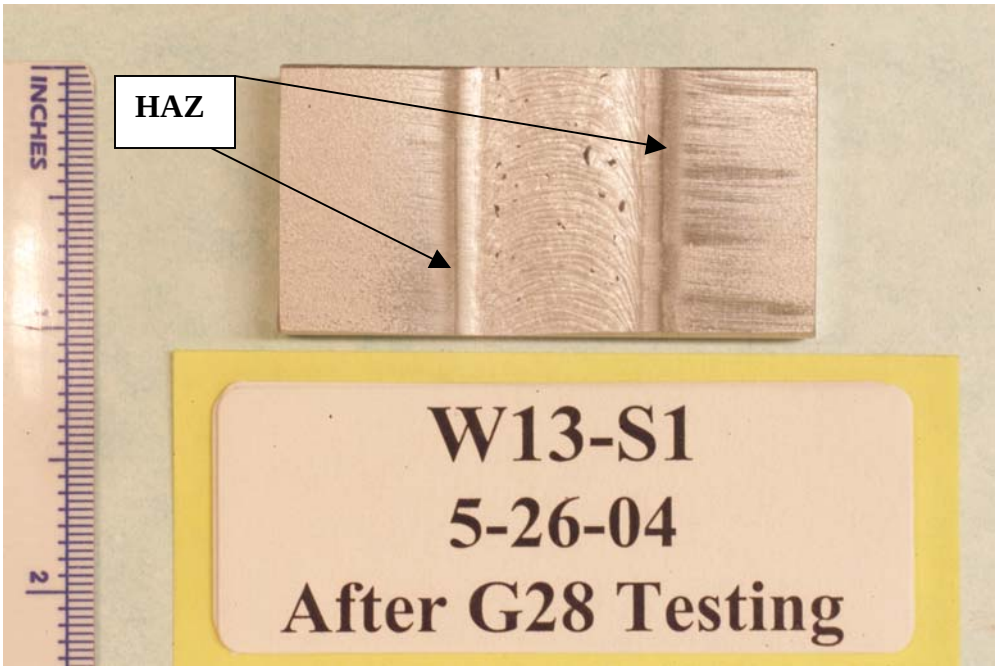

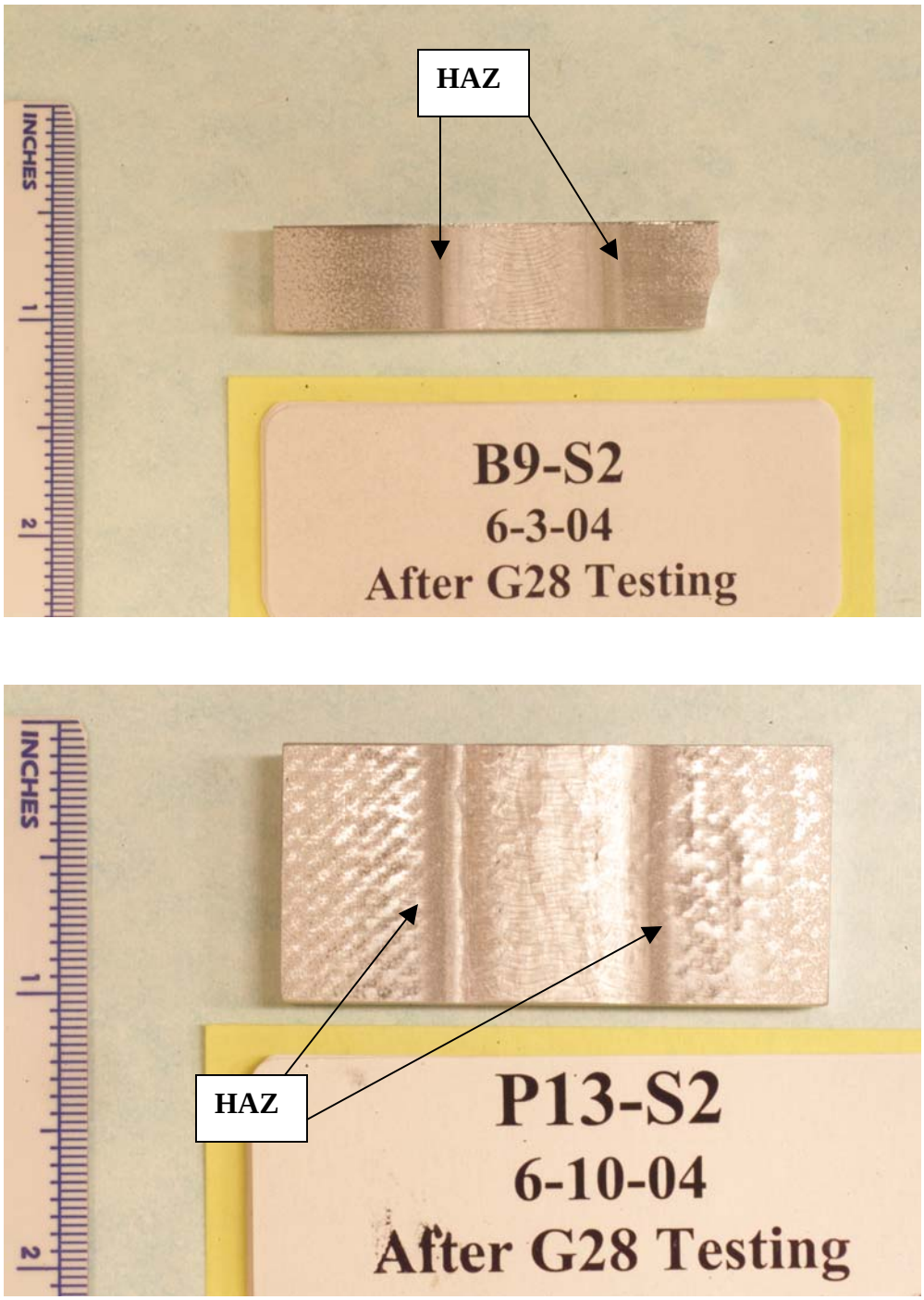

FIGURE 2 - General Appearance of Typical Coupons after the Tests.
The darker stripes at both sides of the weld seam are the IGA of the HAZ.
The identification of the coupons is given in Table 2

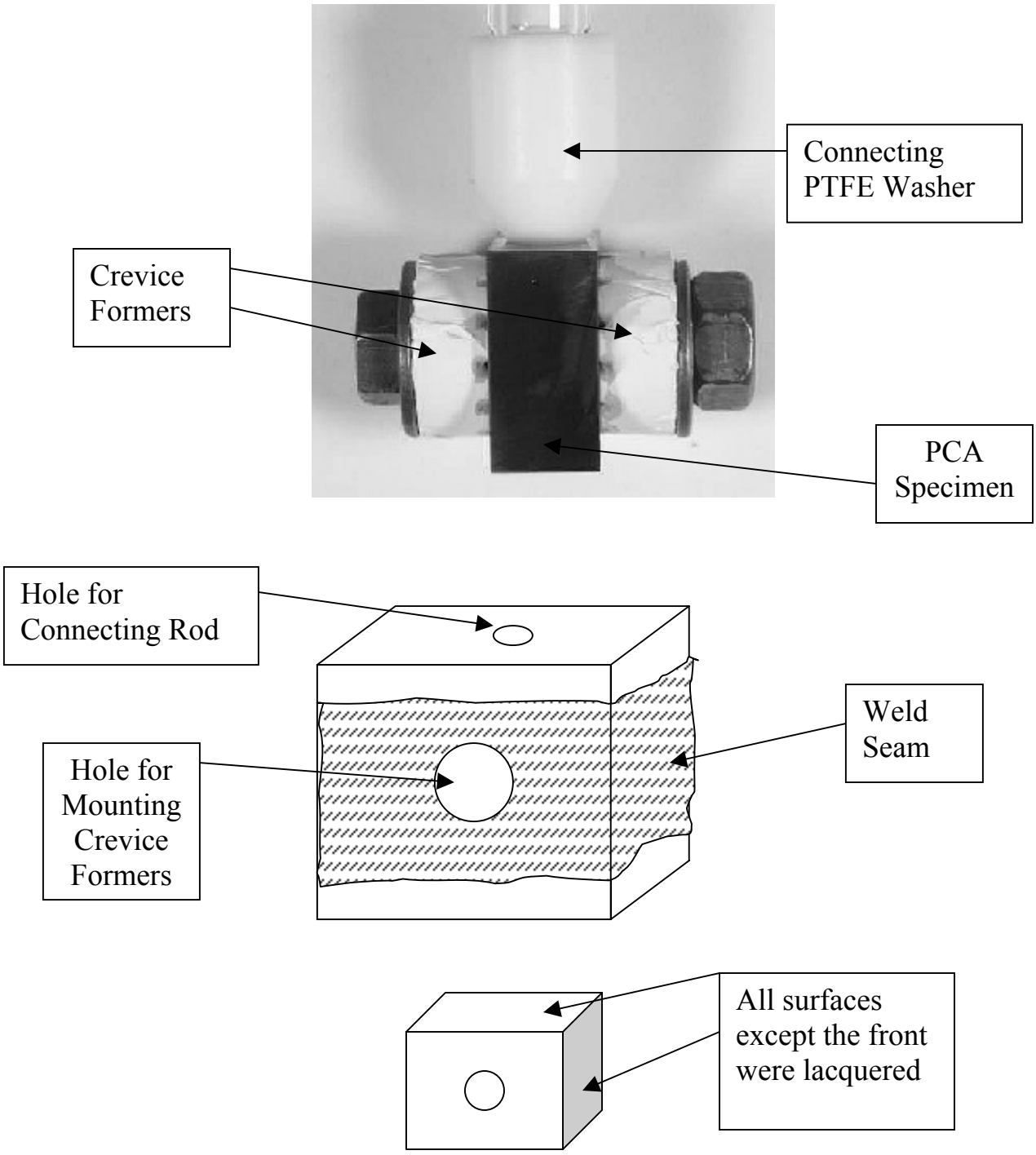

FIGURE 3 - PCA Specimen (0.75 x 0.75 x 0.375 inch or approx. 20 x 20 x 10 mm).
The exposed surface area for testing was 3.27 cm².

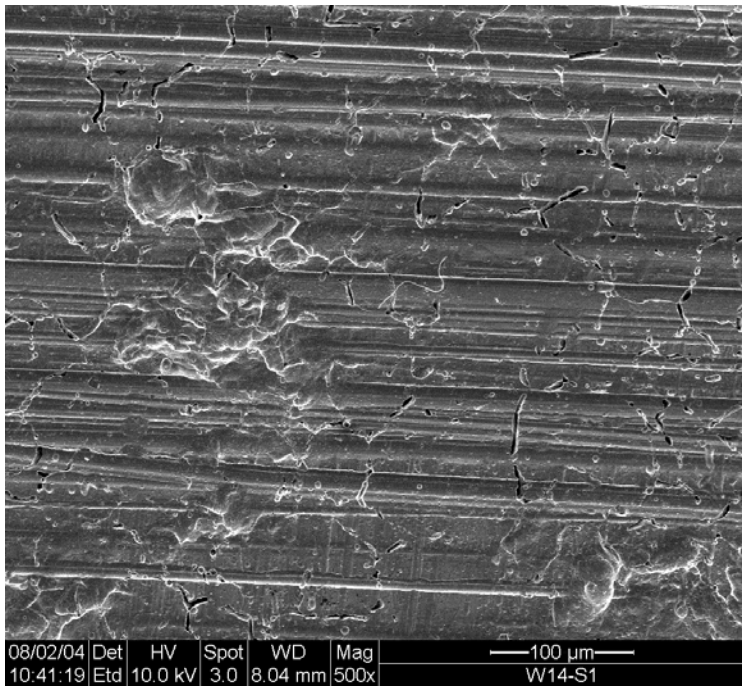

FIGURE 4 - SEM Image of ASW Coupon W14-S1 showing IGA in the base metal away from the weld seam. Magnification X 500

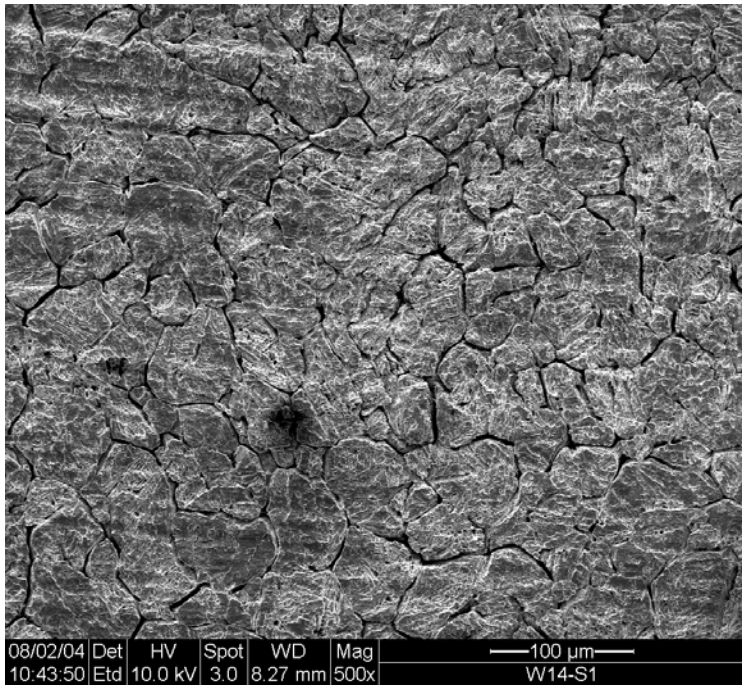

FIGURE 5 - SEM Image of ASW Coupon W14-S1 showing IGA in the base metal in the HAZ area. Magnification X 500

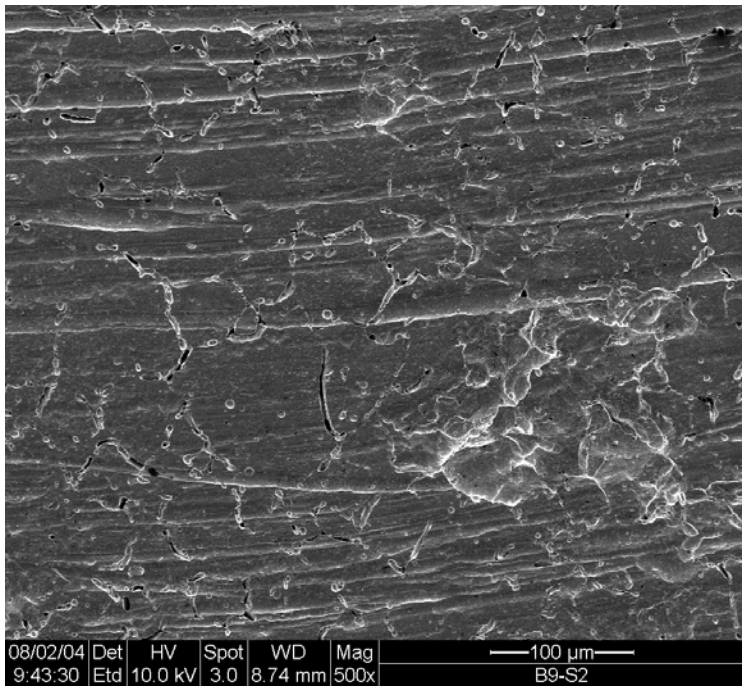

FIGURE 6 - SEM Image of LPB Coupon B9-S2 showing IGA in the base metal away from the weld seam. Magnification X 500

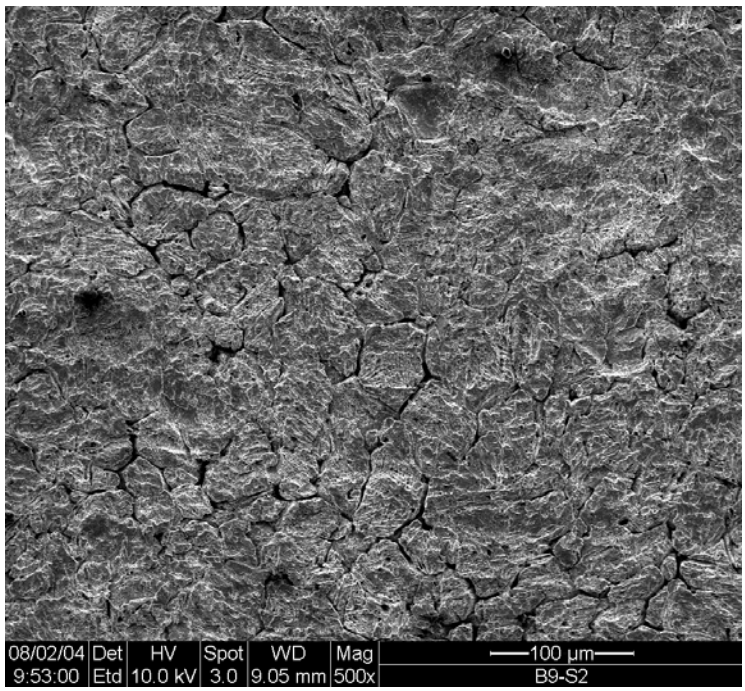

FIGURE 7 - SEM Image of LPB Coupon B9-S2 showing IGA in the base metal in the HAZ area. Magnification X 500

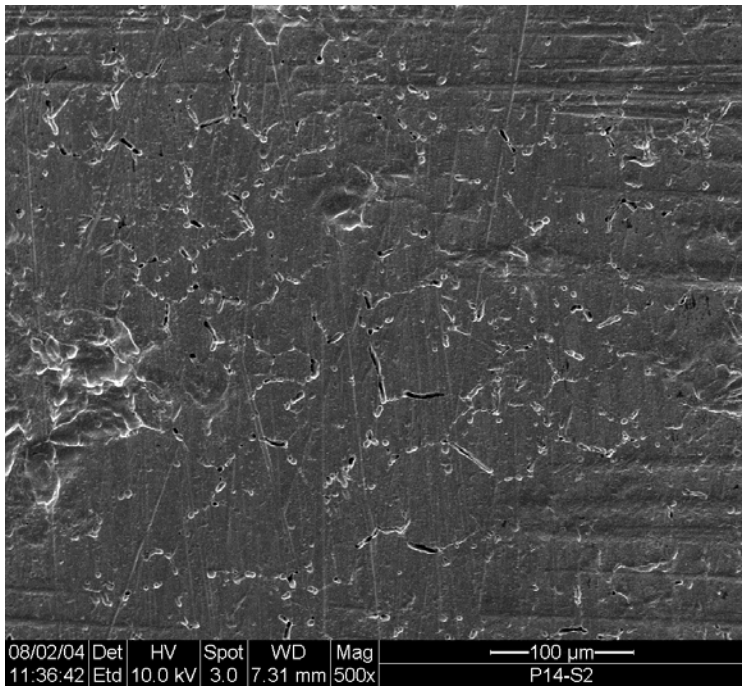

FIGURE 8 - SEM Image of LSP Coupon P14-S2 showing IGA in the base metal away from the weld seam. Magnification X 500

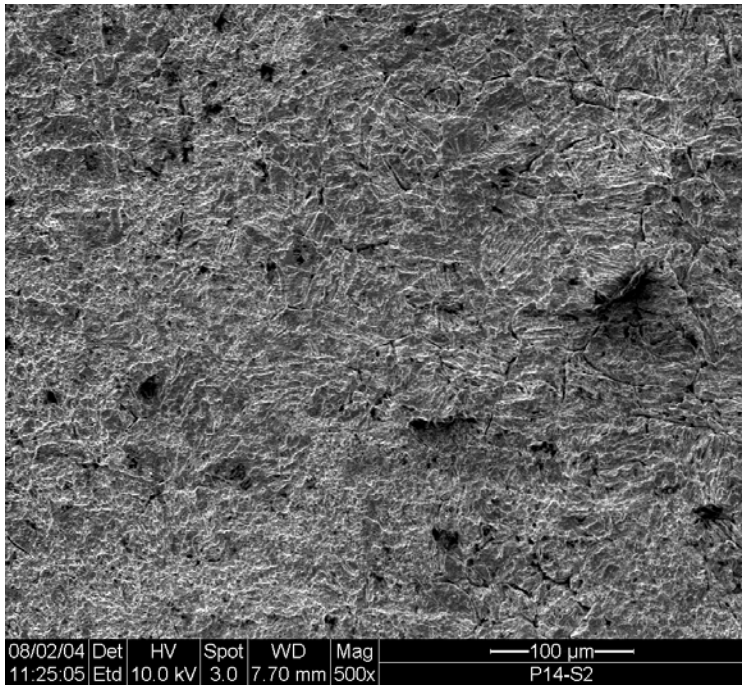

FIGURE 9 - SEM Image of LSP Coupon P14-S2 showing IGA in the base metal in the HAZ area. Magnification X 500

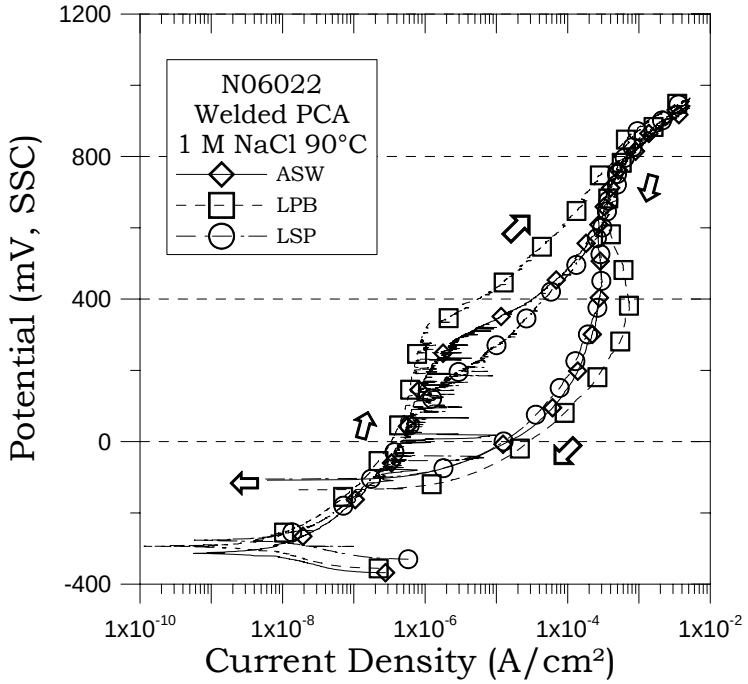

FIGURE 10 - CPP of Alloy 22 in 1 M NaCl at 90°C.
Similar behavior found for ASW, LPB and LSP materials

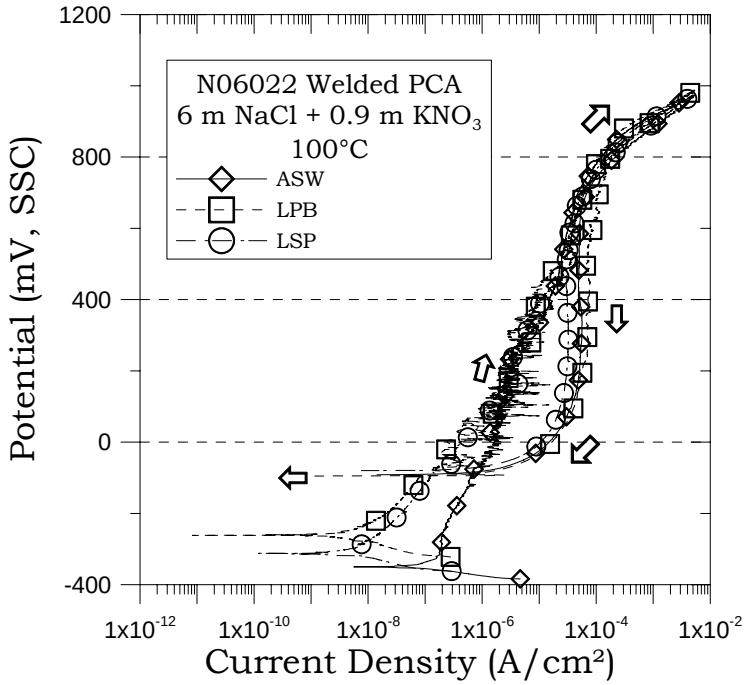

FIGURE 11 - CPP of Alloy 22 in 1 M NaCl at 90°C.
Similar behavior found for ASW, LPB and LSP materials

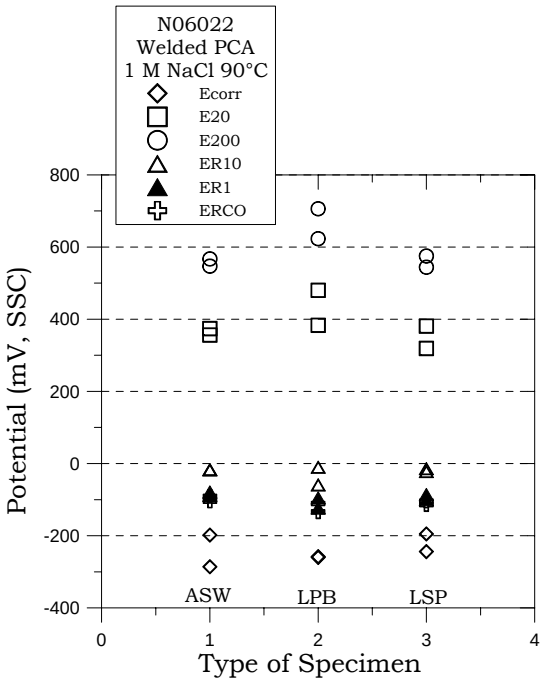

FIGURE 12 - Characteristic Potentials from CPP Curves for the three N06022 Materials in 1 M NaCl at 90°C.

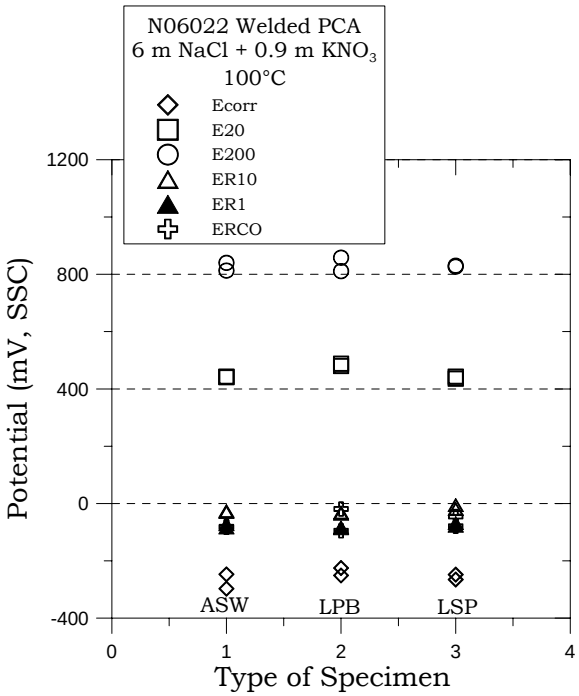

FIGURE 13 - Characteristic Potentials from CPP Curves for the three N06022 Materials in 6 m NaCl + 0.9 m KNO_3 at 100°C

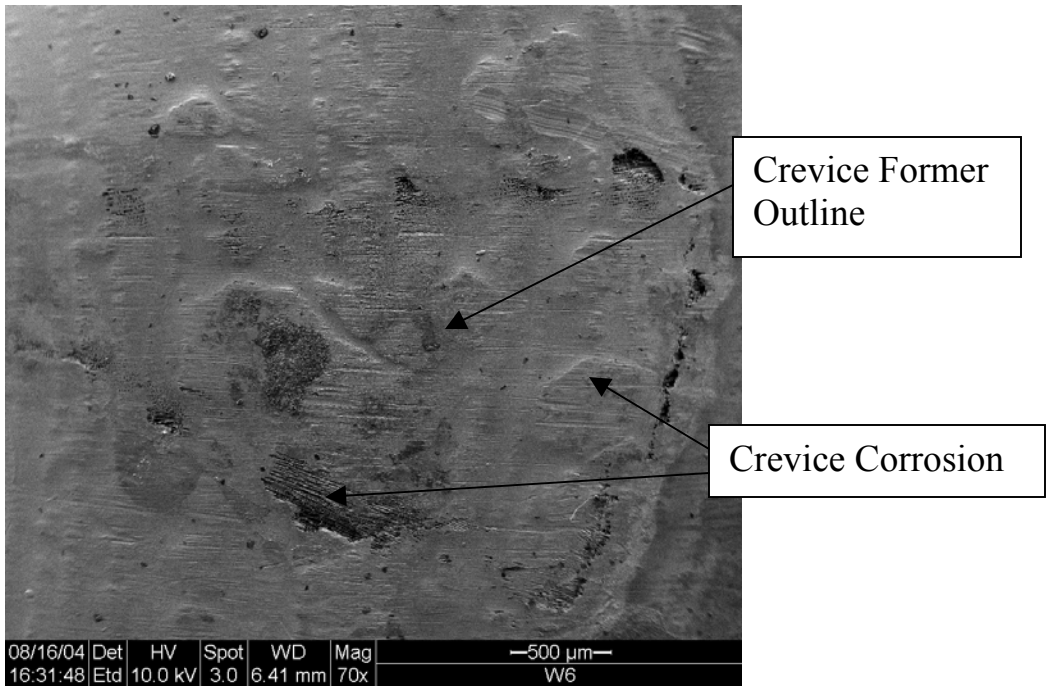

FIGURE 14 - SEM image of ASW Specimen W6 Tested in 1 M NaCl at 90°C. The surface does not appear flat. Magnification X 70

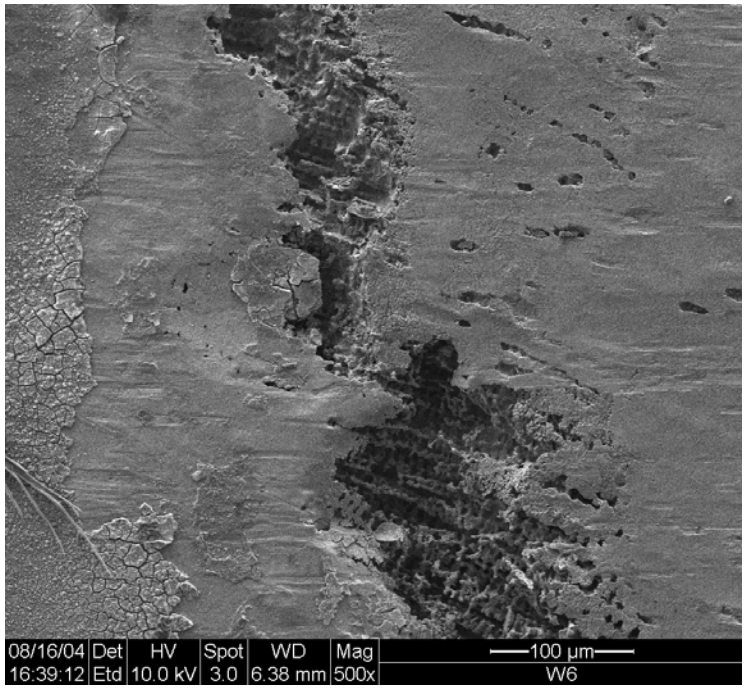

FIGURE 15 - SEM image of ASW Specimen W6 Tested in 1 M NaCl at 90°C. Crevice Attack is Interdendritic. Magnification X 500

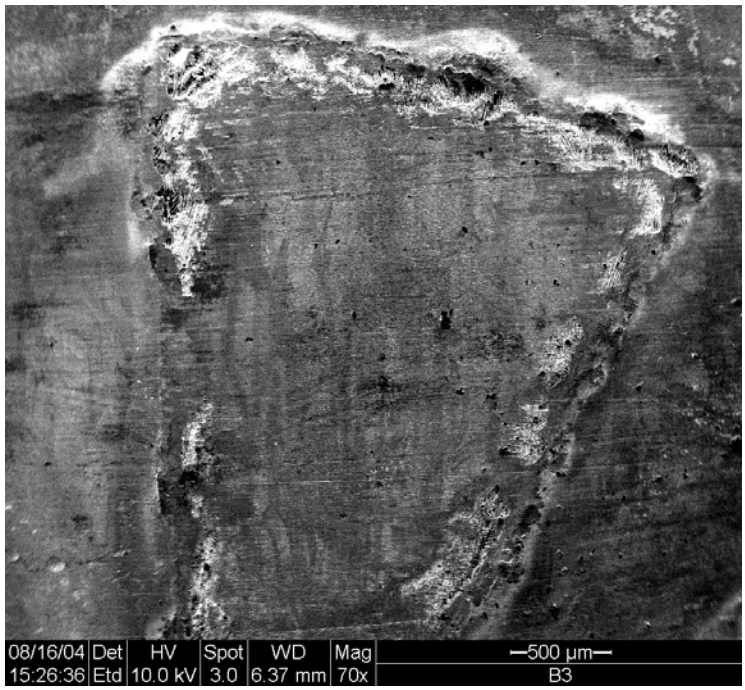

FIGURE 16 - SEM image of LPB Specimen B3 Tested in 1 M NaCl at 90°C. The surface does not appear flat. Magnification X 70

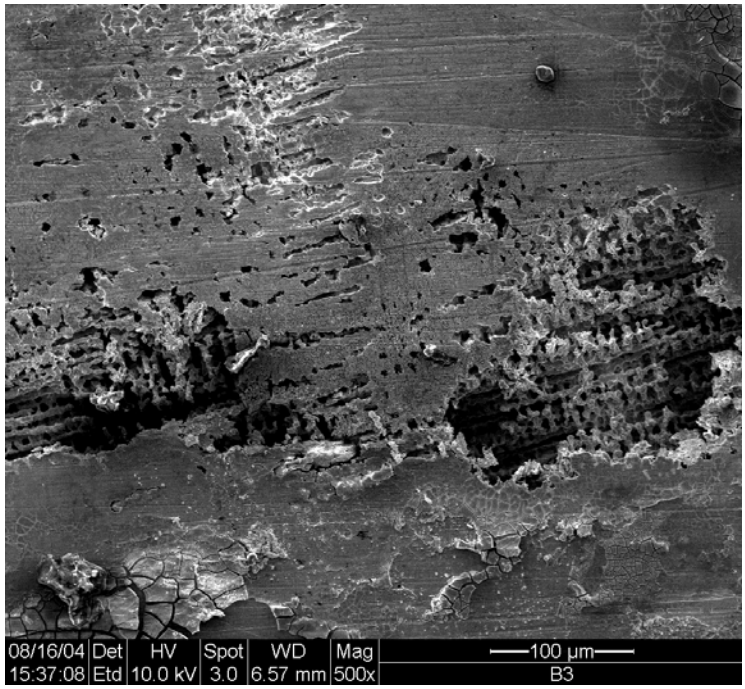

FIGURE 17 - SEM image of LPB Specimen B3 Tested in 1 M NaCl at 90°C. Crevice Attack is interdendritic. Magnification X 500

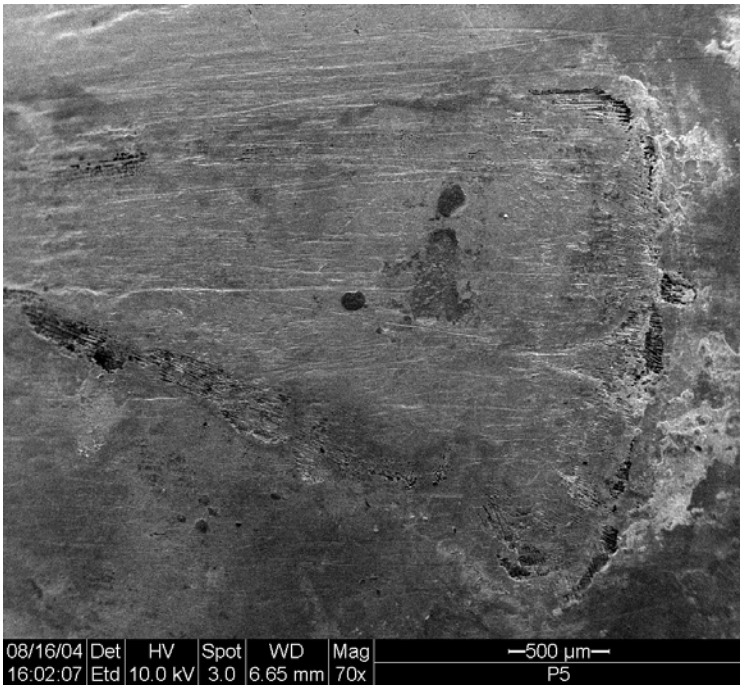

FIGURE 18 - SEM image of LSP Specimen P5 Tested in 1 M NaCl at 90°C. The surface does not appear flat. Magnification X 70

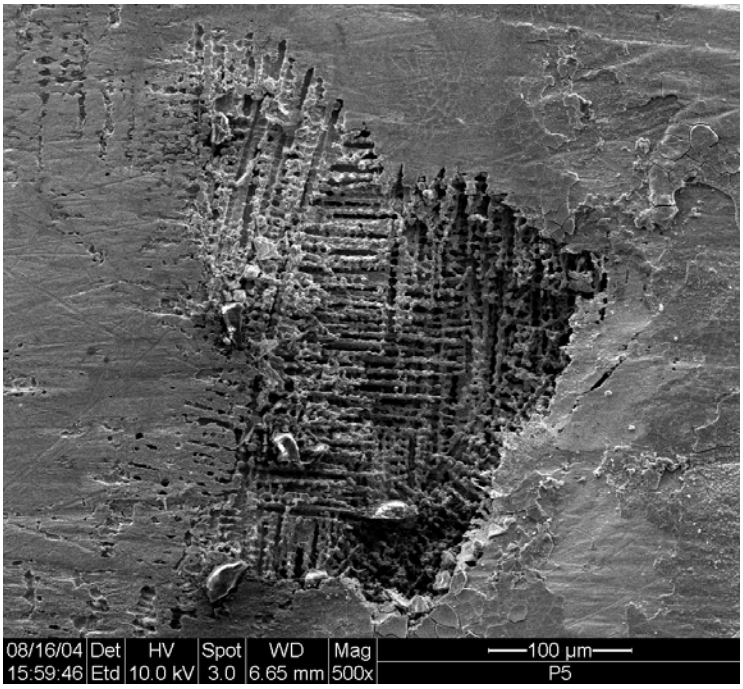

FIGURE 19 - SEM image of LSP Specimen P5 Tested in 1 M NaCl at 90°C. Crevice Attack is interdendritic. Magnification X 500